JACS
JOURNAL OF THE AMERICAN CHEMICAL SOCIETY

Article

pubs.acs.org/JACS

Phenalenone Polyketide Cyclization Catalyzed by Fungal Polyketide Synthase and Flavin-Dependent Monooxygenase

Shu-Shan Gao,[†] Abing Duan,[‡] Wei Xu,[†] Peiyuan Yu,[‡] Leibniz Hang,[‡] K. N. Houk,*[,‡] and Yi Tang*[,†,‡]

[†]Department of Chemical and Biomolecular Engineering and [‡]Department of Chemistry and Biochemistry, University of California, Los Angeles, California 90095, United States

Supporting Information

ABSTRACT: Phenalenones are polyketide natural products that display diverse structures and biological activities. The core of phenalenones is a peri-fused tricyclic ring system cyclized from a linear polyketide precursor via an unresolved mechanism. Toward understanding the unusual cyclization steps, the *phn* biosynthetic gene cluster responsible for herqueinone biosynthesis was identified from the genome of *Penicillium herquei*. A nonreducing polyketide synthase (NR-PKS) PhnA was shown to synthesize the heptaketide backbone and cyclize it into the angular, hemiketal-containing naphtho-γ-pyrone prephenalenone. The product template (PT) domain of PhnA catalyzes only the C4−C9 aldol condensation, which is unprecedented among known PT domains. The transformation of prephenalenone to phenalenone requires an FAD-dependent monooxygenase (FMO) PhnB, which catalyzes the C2 aromatic hydroxylation of prephenalenone and ring opening of the γ-pyrone ring simultaneously. Density functional theory calculations provide insights into why the hydroxylated intermediate undergoes an aldol-like phenoxide−ketone cyclization to yield the phenalenone core. This study therefore unveiled new routes and biocatalysts for polyketide cyclization.

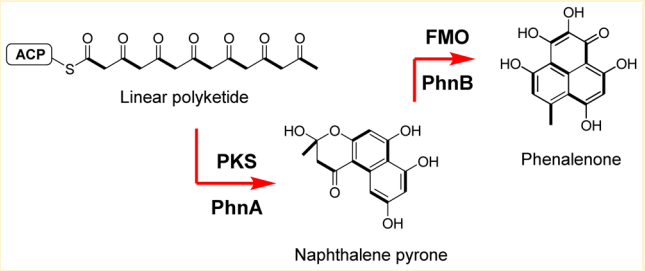

INTRODUCTION

Fungal aromatic polyketides constitute a large group of natural products with diverse biological activities toward plants, animals, and humans, ranging from beneficial, such as the antifungal griseofulvin, to the carcinogenic aflatoxin.[1] The polycyclic core of aromatic polyketides is formed from a cascade of well-controlled intramolecular cyclization reactions starting with a poly-β-keto-thioester backbone, which is synthesized from malonyl-CoA by nonreducing polyketide synthases (NR-PKSs).[2] NR-PKSs are megasynthases that contain linearly juxtaposed catalytic domains that typically include SAT (starter-unit:ACP transacylase),[3] KS (β-ketosynthase), MAT (malonyl-CoA:ACP transacylase), PT (product template),[4] ACP (acyl-carrier protein),[5] and TE/CLC (thioesterase/Claisen-like cyclase)[6] (Figure 1). Following formation of the reactive poly-β-ketone chain by the collective functions of KS, MAT, and ACP domains, the PT domain is responsible for the regioselective intramolecular aldol condensation steps that form the first (and sometimes accompanied by the second) aromatic rings.[4,7] Different cyclization regioselectivities for the first ring cyclization (e.g., C2−C7, C4−C9, C6−C11, and C8−C13[8]) by individual PT domains give rise to the structural diversity observed among fungal aromatic polyketides. Following the actions of the PT domain, the terminal TE/CLC domain can further catalyze Claisen-like condensation reactions that form additional rings and also release the polyketide product that is attached as a thioester on the ACP domain of the megasynthase.[6,9] Interestingly, all NR-PKSs characterized to date produce linearly fused, aromatic compounds, including naphthoxanthone (SMA76a[10]), anthraquinone (norsolorinic acid[7c]), naphtho-γ-pyrone (YWA1,[6] **1**), etc. (Figure 1A). The activities of the corresponding PT and TE/CLC domains have been well-studied, establishing sequence−activity relationships that have enabled NR-PKS product prediction and engineering.[7a,b,11]

In contrast to nearly all biosynthetically characterized fungal aromatic polyketides, the phenalenone family of compounds contain a "nonlinearly" cyclized tricyclic core in which a benzene ring is peri-fused to a naphthalene.[12] The core is heavily derivatized and oxidized to afford structurally diverse natural products and significant biological activities, including the antibacterial (+)-deoxyherqueinone **2** and herqueinone **3** and the anticancer duclauxin **4** (Figure 1B), as well as numerous derivatives shown in Figure S1 of the Supporting Information (SI).[13] *Penicillium herquei* and related fungal strains are prolific producers of phenalenones, and compounds from fermentation of *P. herquei* have been reported to treat tumors, bacterial infections and/or mycoses, and rheumatic diseases.[14] Isotope-feeding studies have confirmed that the phenalenone core of **3** is derived from seven acetate units (heptaketide) and therefore should be catalyzed by a NR-PKS (Figure 1C).[15] Following formation of the cyclized polyketide core, phenalenones are presumed to be modified by post-PKS

Received: February 10, 2016
Published: March 15, 2016

DOI: 10.1021/jacs.6b01528
J. Am. Chem. Soc. 2016, 138, 4249−4259

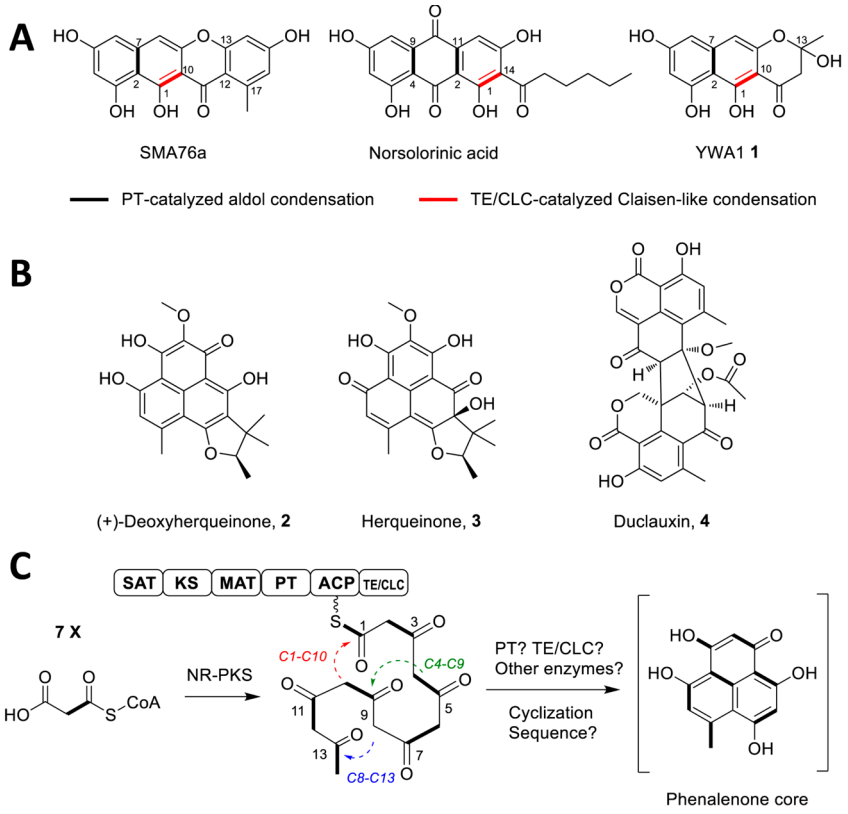

Figure 1. Aromatic polyketides from fungi. (A) Linear aromatic polyketides synthesized by fungal NR-PKS, in which PT and TE/CLC domains control the aromatic cyclization regioselectivity. (B) Phenalenones isolated from various fungal species including *P. herquei*. See Figure S1 (SI) for more examples. (C) Proposed cyclization steps required to form the phenalenone core. See Figure S2 (SI) for more details regarding the possible order of cyclization events. Each thick bond indicates an intact acetate unit.

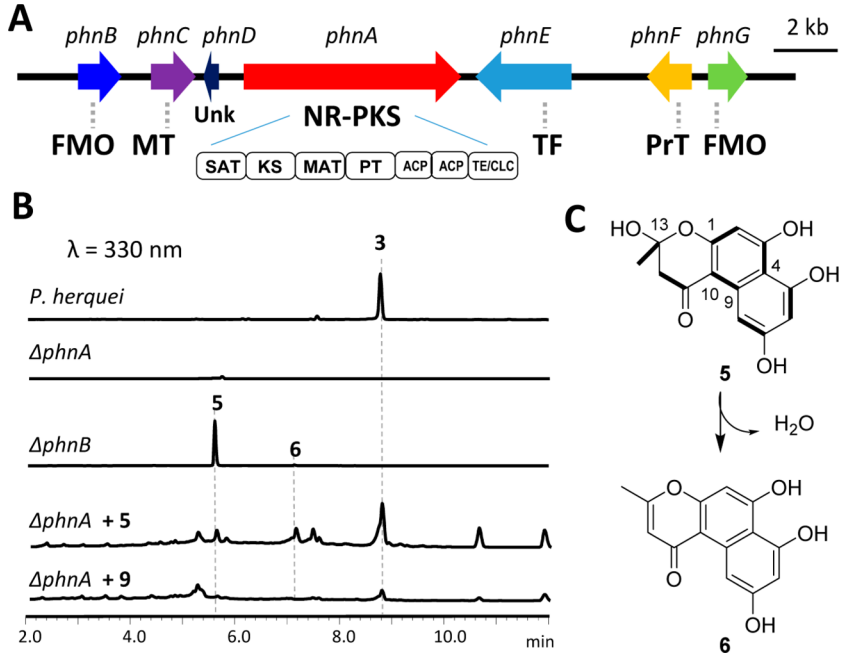

Figure 2. The *phn* gene cluster from *P. herquei*. (A) Organization and proposed function the *phn* gene cluster; TF = transcriptional factor. (B) LC–MS analysis of organic extracts obtained from the wild type, different single-gene knockout mutants, and chemical complementation studies. (C) Structures of the naphtho-γ-pyrone product **5** from the NR-PKS PhnA and the dehydration product **6**. Each thick bond in **5** indicates an intact acetate unit.

tailoring enzymes, including those responsible for C2 hydroxylation and O-methylation, prenylation and formation of the fused furan ring, and other transformations, to generate the final natural products.[12,16]

DOI: 10.1021/jacs.6b01528
J. Am. Chem. Soc. 2016, 138, 4249–4259

The ^{13}C-labeling patterns of **3** from feeding studies suggest that the phenalenone core is formed through a unique combination of three regioselective cyclization steps,[15] including one aldol-condensation step that connects either C4−C9 or C8−C13, a Claisen-like condensation step that connects C1−C10 and releases the polyketide, and an additional aldol-like C−C bond-forming step between either C8−C13 or C4−C9, whichever is not formed in the first aldol condensation step (Figure 1C). To date, all C−C bond-forming steps during cyclization of linearly fused aromatic polyketides are between an enolate and a carbonyl in uncyclized portions of the polyketide chain.[2] In contrast, to generate the peri-fused ring system in phenalenones, regardless of the order of the three cyclization steps, we propose that one of the carbon−carbon bond formation steps (C8−C13 or C4−C9) requires generation of a phenoxide nucleophile from a previously cyclized aromatic ring (Figure S2, SI). Hence to complete this cascade of cyclization reactions on a heptaketide precursor, the PT and TE/CLC domains must possess features that are unique compared to those involved in the formation of the linearly fused products, and/or other partnering enzymes may be involved as well. Elucidating the biochemical basis of the phenalenone cyclization steps can therefore increase our understanding of fungal aromatic polyketide biosynthesis and ability for biosynthetic engineering.

In this study, we report the identification of the *phn* biosynthetic gene cluster from *P. herquei* and the biochemical characterization of the NR-PKS PhnA involved in phenalenone biosynthesis. We show that PhnA synthesizes a novel angular naphtha-γ-pyrone product that is oxidatively morphed into the phenalenone structure by a flavin-dependent monooxygenase (FMO) PhnB. Through density functional theory (DFT) calculations, we propose a mechanism for the reaction. The combined activities of PhnA and PhnB represent a new strategy of polyketide cyclization in nature.

RESULTS

Identification of the *phn* Biosynthetic Gene Cluster and the PhnA NR-PKS. We first confirmed the production of phenalenones from *P. herquei* (NRRL 1040). Herqueinone **3** was observed as the major product following 2 days of cultivation on potato dextrose agar (PDA) for 2 days (Figure 2B). The compound was purified and structurally verified to be **3** when compared to literature reports (Figures S7, S24, and S25, SI).[17] The 33 Mb draft genome of *P. herquei* was then obtained using Illumina HiSeq 2000 sequencing and assembled and annotated using SOAPdenovo.[18] Bioinformatic analysis using antiSMASH[19] revealed the organism to encode 10 biosynthetic gene clusters that may contain a NR-PKS (Table S2, SI). We identified one putative gene cluster on contig 424 56.6 that may be responsible for the biosynthesis of **3** (Figure 2A and Table S3, SI). In addition to an encoded NR-PKS (PhnA), which has the domain architecture of SAT-KS-MAT-PT-ACP-ACP-TE/CLC, neighboring genes encode FMO (PhnB and PhnG), *O*-MT (PhnC), and prenyltransferase (PrT, PhnF) that are consistent with the structural features of **3**. Reverse-transcription polymerase chain reaction analysis showed that transcription of the *phn* genes is synchronized with the production of **3** in *P. herquei* (Figure S3, SI). To confirm the involvement of *phnA* in the biosynthesis of **3**, we performed genetic knockout of the KS region of *phnA* using homologous recombination and hygromycin as selection marker (Figure S4, SI). Deletion of *phnA* completely abolished the production of **3** (Figure 2B), thereby establishing the link between the *phn* cluster and biosynthesis of **3** in *P. herquei*.

Functional Characterization of the *phn* NR-PKS PhnA. To identify the polyketide product of PhnA and the functions of its cyclization domains, the intronless *phnA* was cloned under ADH2 promoter on a 2 μ plasmid and transformed into the engineered *Saccharomyces cerevisiae* strain BJ5464-NpgA.[20] After 3 days of culturing, the yeast culture exhibits a darker brown color not observed with the control strain. LC−MS analysis of the extracted metabolites showed accumulation of a new compound, **5** (*m*/*z* 277 [M + H]$^+$, Figures 3 and S8, SI),

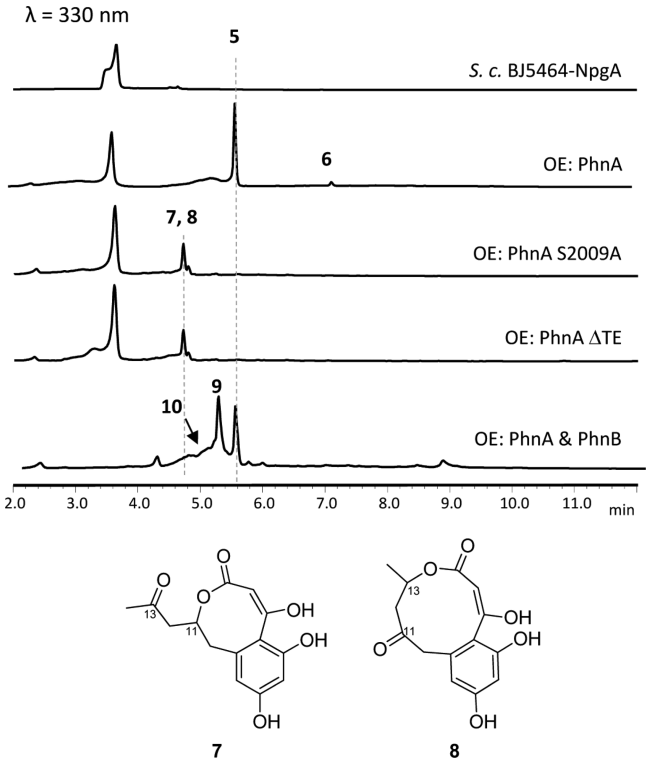

Figure 3. LC−MS analysis of metabolites produced from yeast culture expressing different *phn* enzymes. PhnA alone produced the naphtho-γ-pyrone **5**, while addition of PhnB produced phenalenone **9**. When the TE domain of PhnA was inactivated either by point mutation or domain deletion, the shunt products **7** and **8** were observed in yeast. The reduction of either C11 or C13 ketone to the hydroxyl groups are likely performed by endogenous yeast ketoreductases, as purified PhnA mutants did not produce the same compounds in vitro. The peak at ∼3.5 min is 2-methylbenzoic acid, which is a yeast metabolite.

and a minor product, **6** (*m*/*z* 259 [M + H]$^+$, Figure S9, SI). Both **5** and **6** were isolated from yeast (5 and 0.3 mg/L, respectively) and the structures were determined by extensive NMR analysis (Table S6, Figures S26−S34, SI). Both compounds are heptaketide products with a tetrahydroxylnaphthalene (THN) core angularly fused to a γ-pyrone ring. While the pyrone ring in **5** (named prephenalenone) contains a hemiketal that is formed upon attack of the C1 hydroxyl group on the C13 ketone, **6** exists as a mixture of two interconverting tautomers that form after dehydration of **5** (Figures 2C and S9, SI). The dehydration occurs spontaneously under aqueous and room temperature conditions within 48 h (Figure S14A, SI), which was similarly observed for the conversion of the linear naphthopyrone YWA1 **1** into nor-rubrofusarin even in the absence of a dedicated dehydratase.[21] To test whether **5** is an

DOI: 10.1021/jacs.6b01528
J. Am. Chem. Soc. 2016, 138, 4249−4259

on-pathway intermediate in the biosynthesis of **3**, purified **5** was added to the Δ*phnA*-blocked mutant at 50 mg/L. LC−MS analysis of the culture after 72 h showed that production of **3** was restored while minor conversion to **6** was observed (Figure 2B). In contrast, chemical complementation of Δ*phnA* using **6** did not restore the production of **3**.

To demonstrate that PhnA is the enzyme required to synthesize **5**, recombinant PhnA (237 kDa) was purified from yeast to homogeneity and assayed in the presence of 2 mM malonyl-CoA in vitro (Figure S5, SI). The predominant product of the assay was indeed confirmed to be **5** upon LC−MS analysis, with a small amount of **6** present (Figure 4). Repeating the assay using [2-^{13}C]malonyl-CoA that is generated in situ from [2-^{13}C]malonate, coenzyme A, and MatB[22] showed an increase in the mass of **5** by seven mass units (*m*/*z* 282 $[M - H]^-$), consistent with the heptaketide backbone of **5** (Figure S15, SI). Hence, PhnA is solely responsible for the production of **5**, which must be derived from an uncyclized heptaketide precursor via the sequential cyclization of C4−C9 by aldol condensation and C1−C10 Claisen-like condensation to generate the THN intermediate **12**, followed by attack of C1-OH on C13 to form the naphtho-γ-pyrone (Figure 5). This sequence of cyclization events is parallel to that involved in the formation of the linearly fused **1** with key differences in regioselectivities of the first aldol-condensation step (C2−C7 instead of C4−C9) (Figure 5).[6]

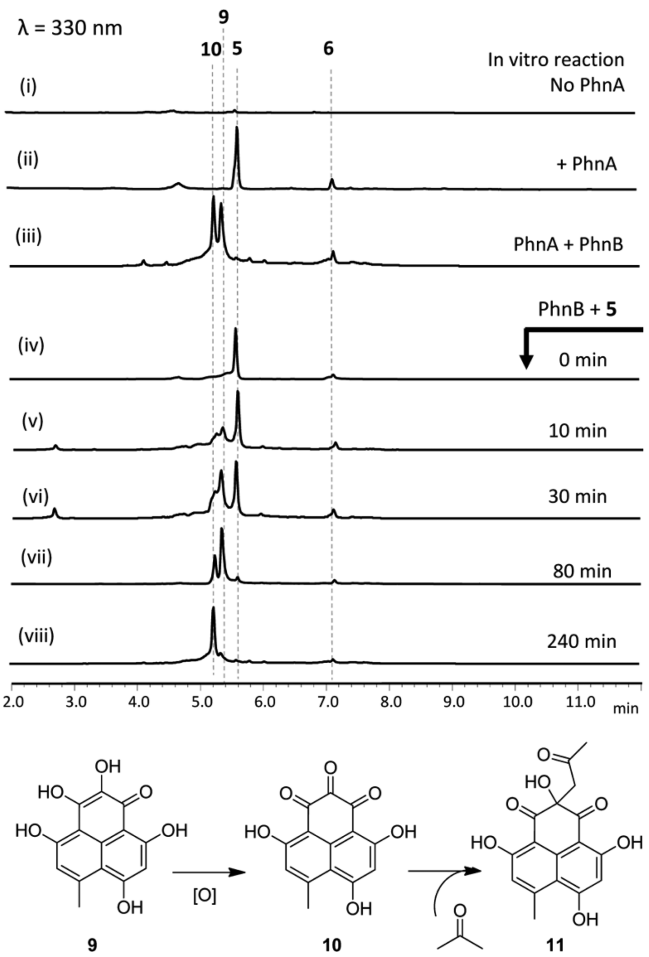

Figure 4. LC−MS analysis of compounds produced from assays containing purified enzymes. (i) Control reaction without PhnA. (ii) Reaction catalyzed by 5 μM PhnA in the presence of 100 mM potassium phosphate buffer (pH 7.9) and 2 mM malonyl-CoA. (iii) Reaction catalyzed by 5 μM PhnA and 20 μM PhnB in the presence of 100 mM potassium phosphate buffer (pH 7.9), 2 mM malonyl-CoA, 20 μM FAD, and 4 mM NADPH. Reactions in i−iii were extracted after overnight incubation at 25 °C. (iv−viii) Time course analysis of 5 μM PhnB catalyzed conversion of **5** to **9** (and the oxidation of **9** to **10**). In vitro reaction conditions are 100 mM potassium phosphate buffer (pH 7.9), 20 μM FAD, 4 mM NADPH, and 1 mM **5**.

Delineating the Roles of PT and TE/CLC of PhnA. While PT-catalyzed C4−C9 cyclization of polyketides was previously observed in the formation of norsolorinic acid and nor-toralactone (Figure 5), the first ring cyclization steps are always accompanied by the consecutive C2−C11 aldol condensation that is likely also catalyzed by the respective PT domains.[7c,23] Hence, a PT domain that performs only a single C4−C9 aldol condensation as required in the formation of **5** has not been previously reported. To investigate the role of the PT domain, as well as the TE/CLC domain, we constructed two version of PhnA that is inactivated in the TE/CLC domain (PhnA TE^0).[9a] Both the active site serine to alanine mutant (S2009A) and the TE deletion (ΔTE) versions of PhnA were expressed in BJ5464-NpgA, followed by metabolite analysis, as shown in Figure 3. LC−MS analysis showed that both mutants lost the ability to produce **5** and **6**, but instead, two new compounds with the same mass (*m*/*z* 279 $[M + H]^+$) accumulated, **7** and **8**. Both compounds were isolated from yeast culture (2 mg/L for **7**, Figure S10; 0.4 mg/L for **8**, Figure S11, SI) and their structures were elucidated by NMR analysis (Table S7 and Figures S35−S44, SI). Both new compounds featured a bicyclic system in which the 1,3-dihydroxybenzene ring is fused to either an 8-membered (**7**) or a 10-membered (**8**) macrolactone. Compared to **5**, it is evident that while the TE/CLC mutation abolished the second aromatic ring in **5** that is derived from the C1−C10 Claisen condensation, the first aromatic ring that is fixed from C4−C9 aldol condensation remained intact. This confirms that the PT domain in PhnA is only responsible for directing the C4−C9 cyclization, while the TE/CLC domain catalyzes the C1−C10 cyclization. Formation of the macrolactones **7** and **8** requires ketoreduction of the C11 and C13 carbonyl groups, respectively, and the subsequent attack by the hydroxyl groups on the C1 thioester (Figure 5). We propose that the ketoreduction steps are catalyzed by endogenous yeast ketoreductases, as observed previously with other ketone-containing compounds.[24] Mutation in the PhnA TE/CLC domain inactivates the release of **12** and stalls the resorcinol-containing thioester intermediate on the ACP domain. This stalling likely enables access of the ketone groups by yeast KR enzymes and leads to macrolactone formation. To verify that the reduction activities do not reside in PhnA, both TE^0 mutants were purified from yeast and assayed in the presence of malonyl-CoA. As expected, no product turnover was observed from the in vitro reactions.

FMO-Catalyzed Formation of Phenalenone. Previous work with WA that produces **1** led to the proposal that formation of the hemiketal may also be promoted by the TE/CLC domain.[6] We explored the energetics of various species involved in their transformation by DFT computations (see the Supporting Information for details). These computations show that the hemiketal **5** is ∼3.7 kcal/mol more stable than the ring-opened diketo-THN **12** (Figure S19, SI). This explains why **12** is not observed during isolation and characterization of **5**. Indeed, the hemiketal γ-pyrone is very stable, even under strongly acidic treatment (10% trifluoroacetic acid in DMSO)

DOI: 10.1021/jacs.6b01528
J. Am. Chem. Soc. 2016, 138, 4249−4259

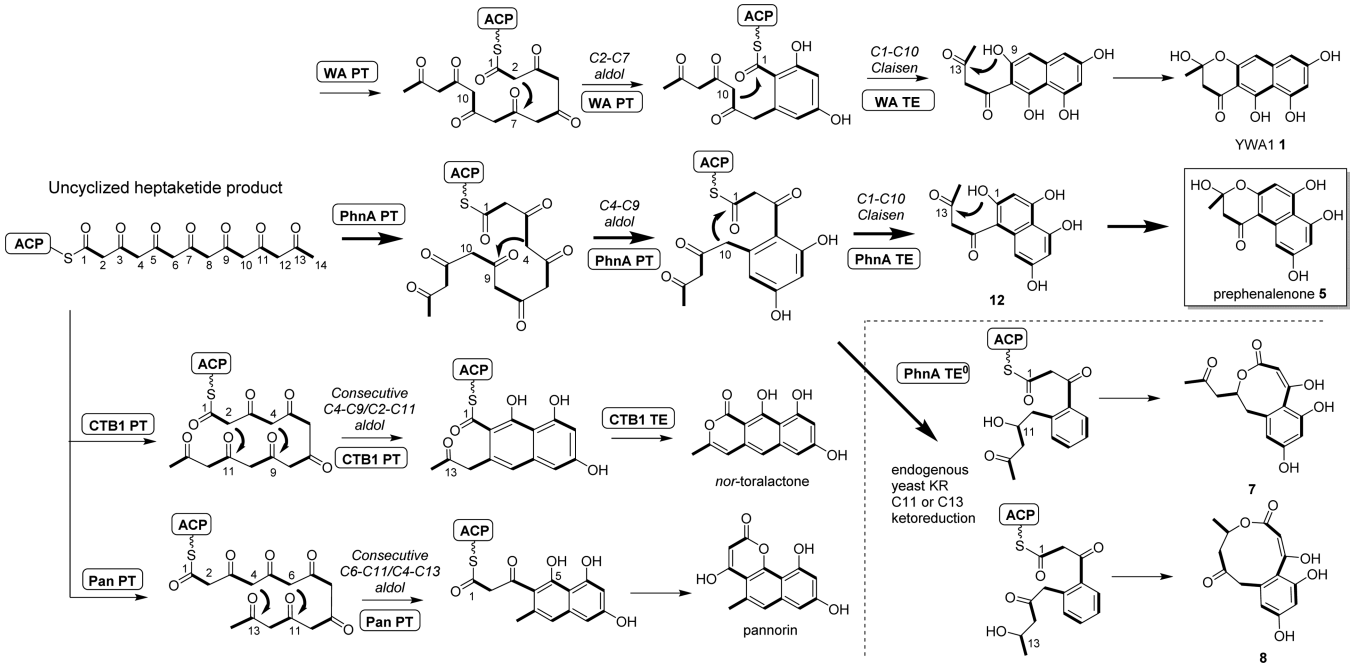

Figure 5. Summary of divergent cyclization regioselectivities of NR-PKSs. All NR-PKSs shown synthesize the common heptaketide precursor that is cyclized into the various final products due to the difference in regioselectivity of the PT domains. The PKS responsible for pannorin biosynthesis is not known and is indicated as Pan for illustration purposes. PhnA PT domain is unique in that it only catalyzes the C4−C9 cyclization, whereas all previously identified PT domains that catalyze C4−C9 cyclization also catalyze the consecutive C2−C11 cyclization, as in CTB1.

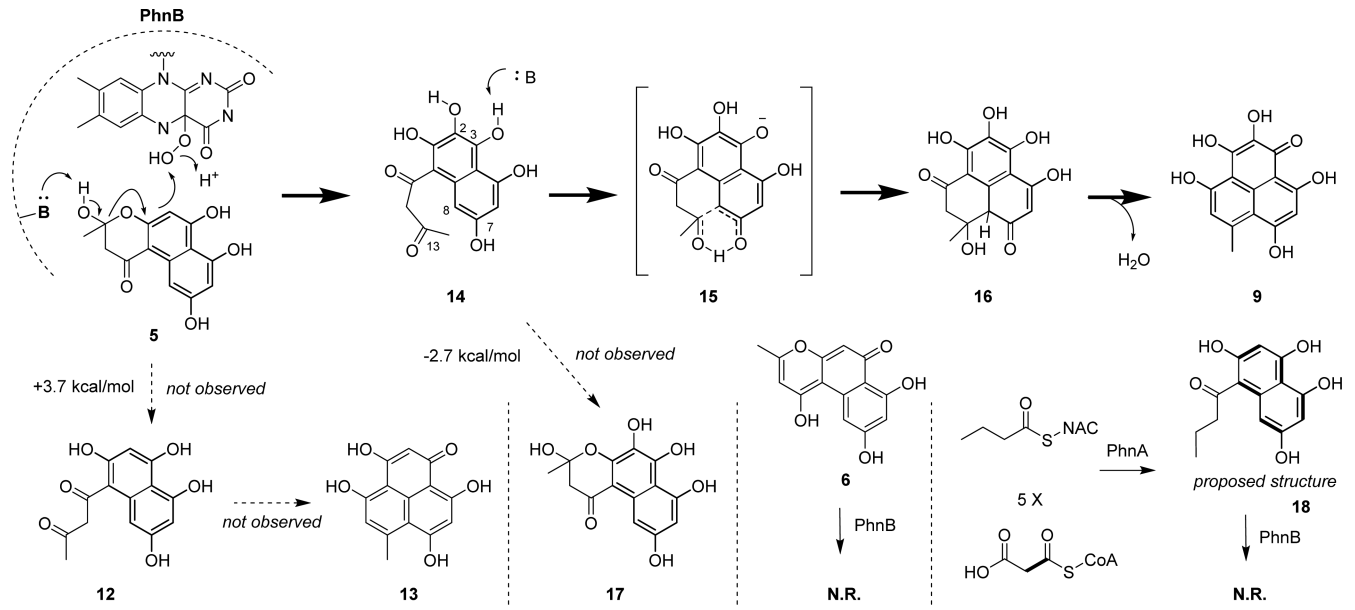

Figure 6. Proposed mechanism for PhnB-catalyzed conversion of **5** to **9**. PhnB catalyzes the C2-hydroxlation of **5** through deprotonation of the hemiketal C13 hydroxyl group to yield **14**. Deprotonation of C3-OH leads to rapid cyclization to form **16**, which can undergo dehydration and aromatization to yield the product **9**. Products that are not observed in the reaction, as well as substrate variants that do not react with PhnB, are indicated.

(Figure S16, SI). Therefore, on the basis of the chemical complementation result that **5** is a biosynthetic precursor of **3**, additional enzyme(s) must be required to open the γ-pyrone ring to facilitate the formation of the last ring (C8−C13 bond formation) to yield a phenalenone product, such as **13** (Figure 6).

To identify the enzyme(s) responsible for pyrone opening and C8−C13 cyclization, we targeted the deletion of selected *phn* genes and sought for the mutant that accumulates **5**. PhnC encodes a small protein (15 kDa) that belongs to the dimeric α/β barrel (Dabb) protein superfamily, including the plant polyketide olivetolic acid cyclase (OAC) that catalyzes a C2−C7 intramolecular aldol condensation.[25] However, deletion of this gene led to only decreased, but not abolished, production of **3**. Meanwhile, structural comparison of all the reported phenalenone-containing fungal natural products showed that the C2 position is invariably oxidized to either a C2-OH (or methoxy) or a C2-keto functional group (Figure 1B).[12] This

DOI: 10.1021/jacs.6b01528
J. Am. Chem. Soc. 2016, 138, 4249−4259

common feature perhaps hinted that the hydroxylation of C2 may somehow be required for the formation of the phenalenone core. To test this hypothesis, we inactivated *phnB*, which encodes a FAD-dependent hydroxylase that has sequence homology to UbiH, the 2-octaprenyl-6-methoxyphenol aromatic hydroxylase in ubiquinone biosynthesis.[26] Interestingly, the Δ*phnB* mutant lost the ability to produce **3**, and **5** accumulated as the predominant product (Figure 2B), hinting that PhnB is the immediate downstream enzyme of PhnA and must play an important role in transforming **5** into a phenalenone structure.

Recombinant PhnB (45 kDa) was expressed and purified from *Escherichia coli* BL21(DE3) as a yellow-hued protein. Addition of PhnB and NADPH to the in vitro assay containing PhnA led to the formation of two new compounds, **9** (m/z 275 $[M + H]^+$) and **10** (m/z 273 $[M + H]^+$), as well as a residual amount of **6** (Figure 4). When 5 μM PhnB was directly added to 1 mM **5** in the absence of PhnA, we observed the rapid conversion of **5** to **9** (complete consumption of **5** in ∼80 min), accompanied by the gradual and eventual complete conversion of **9** to **10**. To determine the structures of **9** and **10**, we coexpressed PhnA and PhnB in BJ5464-NpgA, which led to the accumulation of both **5** and **9** after 3 days of culturing. Workup of the culture showed that most of **9** was found intracellularly and remained intact, which enabled purification and structural elucidation (Figure 3). No trace of **13** (m/z 259 $[M + H]^+$) can be found in the product mixture isolated from the in vitro and in vivo assays involving PhnB, consistent with previous observations that all isolated phenalenones are oxidized at C2.

Purification of **9** proved to be challenging, as it is unstable and prone to conversion into **10** and other products during isolation under room-temperature conditions (Figure S14B, SI). We optimized the conditions and used a low-temperature isolation and purification procedure (see the methods for details) to obtain relatively pure **9** for NMR characterization. Key HMBC correlations from 14-CH_3 to C12, C13, and C8; from H6 to C4, C5, C7, and C8; and from H12 to C8 and C10, C13, and C14 unequivocally established that the structure of **9** contains the intact fused phenalenone core (Table S8 and Figures S45−S48, SI). However, due to tautomerization among C1, C2, and C3 and the lack of additional proton signals, the structure of the northern portion of the molecule could not be fixed, which is also observed for the phenalenone product atrovenetin.[27] However, combining the MS and NMR data, we believe that one form of **9** is indeed the C2-oxidized phenalenone structure, as shown in Figure 4. To determine if **9** is a true intermediate in the biosynthesis of **3**, purified **9** was added to the Δ*phnA* strain. Despite its instability under culturing conditions, we observed restoration of **3** in the chemical complementation experiment, with approximately 5% conversion of **9** (Figure 2B). The conversion of **9** to **10** is spontaneous in air, which suggests that **10** may be the oxidized, triketo product (Figures 4 and S14B, SI). **10** was very unstable and also rapidly degraded during purification. However, **10** could be converted to a stable aldol adduct **11** (m/z 331 $[M + H]^+$) when treated with acetone (Figure S14C, SI), which is a common feature of phenalenones.[12] **11** can be purified, and its structure was established by NMR analysis (Table S8 and Figures S49−S52, SI). The acetone adduct at C2 was unambiguously determined, which supports the structure of **10**, as well as that of the phenalenone core in **9**.

To probe the substrate requirement of PhnB, we first used the dehydrated product **6** as a substrate analogue. No reaction was observed, indicating that the hemiketal and the C13-OH are essential for the C2 hydroxylation activities. This suggests that the C2 hydroxylation is not via the canonical monooxygenase mechanism that involves deprotonation of ortho- or para-substituted phenolic oxygen (such as C3-OH in **5**).[28] We then aimed to generate an uncyclized THN substrate that does not contain a C13 ketone group. To do so, we performed the PhnA in vitro assay using butyryl-SNAC as a starter unit. When presented with the four-carbon primer unit, PhnA synthesized a new product, **18** (m/z 263 $[M + H]^+$), that is derived from a butyryl-primed C18 product (Figure S17, SI). Although this compound was not isolated for structural characterization from the in vitro reaction, on the basis of the mass, number of ketide units from the [2-^{13}C]malonate assay, and the identical UV absorbance to other THN compounds (Figure S18, SI), we can propose that the structure is the butanone-substituted THN, as shown in Figure 6. To probe if PhnB can oxidize the C2 position of **18**, we performed the in vitro assay in the presence of both PhnA and PhnB. No transformation of **18** can be detected (Figure S18, SI), further supporting that PhnB requires the pyrone ring of **5** for catalysis.

Proposed Mechanism of Phenalenone Formation. Our studies show that PhnB is responsible for converting γ-pyrone **5** into the tricyclic phenalenone as well as C2 hydroxylation. These two reactions appear to take place together, since attempts to isolate either C2 hydroxylated γ-pyrone **17** or unhydroxylated phenalenone **13** were unsuccessful. Taking this into consideration, we propose the mechanism of PhnB shown in Figure 6. Following release of the polyketide product from PhnA and rapid formation of the hemiketal **5**, the active site of PhnB initiates the reaction through base-catalyzed deprotonation of C13-OH, which leads to cleavage of the pyrone ring and enables the nucleophilic attack of C2 on the oxidized PhnB Fl-4a-OOH to yield intermediate ketone **14**. Subsequently, deprotonation of the C3-OH group leads to nucleophilic attack of the electron-rich naphthalene ring at C8 on the now accessible C13 ketone to yield the cyclized **16** via the transition state **15**, by intramolecular proton transfer from the C7-OH, which was shown to be facile by computational studies discussed below. This reaction is very fast when the C2-OH is present, which increases the acidity of the C3-OH. Intermediate **16** will aromatize through dehydration and keto−enol tautomerization to yield the phenalenone product **9**.

The purpose and timing of the C2 oxidation are particularly intriguing. Strategically, one can reason that nature incorporated this step (i) to cleave oxidatively the γ-pyrone ring to make the C13 ketone available for C8−C13 bond formation, (ii) to favor possibly electronically the C8−C13 reaction with **14** to yield **16**, or (iii) to serve as the site for downstream tailoring modifications that are important for phenalenone biological activities. It is likely that a combination of all three objectives is achieved in this PhnB-catalyzed reaction. With regard to the second point, the phenalenone cyclization reaction with **14** must occur very rapidly once the C13 carbonyl is exposed, as the competing formation of hemiketal **17** is not observed despite being 2.7 kcal/mol more stable (Figures 6 and S19 and S20, SI). To understand this concerted aldol-like process that forms the third aromatic ring starting from the hemiketal, we performed DFT calculations on the energetics of the cyclization (see the methods for details). In the absence of deprotonation, the aromatic cyclization reaction would be slow at room temperature ($\Delta G^{\ddagger}_{298}$ = 24.4 kcal/mol, starting from **5** via **12** with a computed $t_{1/2}$ (25 °C) = 24 h,

DOI: 10.1021/jacs.6b01528
J. Am. Chem. Soc. 2016, 138, 4249−4259

Figures S19 and S20, SI), but the hydroxylation makes the aromatic cyclization ~50 times faster ($\Delta G^{\ddagger}_{298}$ = 22.1 kcal/mol, starting from **17** via **14**, Figures S19 and S20, SI). The C5-OH of **14** is a more powerful donor when hydrogen bonded to C3−O and stabilizes the enone transition state **15** and the product of the intramolecular aldol-like process (Figures S21 and S22, SI). The calculated slow rate of cyclization prompted us to examine the effect of deprotonation of C3-OH. Starting with either **12** or **14**, calculations show that deprotonation significantly decreases the reaction energy barrier and increases the reaction rate of phenalenone rearrangements [$t_{1/2}$ (25 °C) = 0.018 s for **12** and 0.025 s for **14**] (Figures S21 and S22, SI). In summary, the active site of PhnB provides the general base to perform deprotonation of the more remote hemiketal hydroxyl group in **5** and to cause ring-opening of the pyrone with installation of the C2-OH group in **14**. Subsequent intramolecular deprotonation of C3 phenolic oxygen accelerates phenalenone ring closure to yield **9**.

DISCUSSION

In this paper, we showed that the core of phenalenone polyketides is synthesized by the combined functions of a NR-PKS (PhnA) and a FMO (PhnB) that catalyze an unusual aromatic hydroxylation of the NR-PKS product **5**. Figure 5 is a summary of PT domain regioselectivity in cyclization of heptaketides in fungi. The domain organization of PhnA is identical to that of WA that synthesizes YWA1 (**1**), including the uncommon tandem ACP domains.[6] The two NR-PKSs also share 44% sequence identity and 60% sequence similarity across the entire protein sequence. Both NR-PKSs produce a heptaketide product and catalyze a parallel set of cyclization reactions, including an intramolecular aldol condensation and a C1−C10 Claisen cyclization, to generate the respective naphthopyrone products (Figure 5). The only difference between the two NR-PKSs appears to be in the regioselectivity of the PT domain: whereas the C2−C7 cyclization controlled by WA leads to the linear **1**, the C4−C9 cyclization catalyzed by PhnA results in the angular **5**. The recently characterized CTB1 NR-PKS involved in cercosporin biosynthesis employs a PT domain that catalyzes the tandem C4−C9 and C2−C11 aldol cyclizations in the synthesis of nor-toralactone,[23] functions that are similar to the PT domain of PksA that synthesizes norsolorinic acid.[7c] Our work with PhnA, especially with the isolation of shunt products **7** and **8** from the PhnA TE^0 constructs, unequivocally verifies that the C2−C11 aldol condensation in polyketide cyclization must be catalyzed by the PT domains such as those in CTB1 or PksA, as previously proposed. Hence, the PhnA PT domain is functionally distinct from these C4−C9/C2−C11 PT domains and is unique in that it catalyzes only the C4−C9 cyclization. While the NR-PKS for pannorin has not been discovered to date, the PT domain responsible must catalyzes consecutive C6−C11 and C4−C13 cyclization reactions to set up angular pyrone formation and product turnover, as illustrated in a mix-and-match experiment involving heterologous domain combinations.[11c]

Having identified PhnA PT as a new addition to the PT domain diversity, we sought to compare its sequence to other PT domains using phylogenetic analysis. We previously classified the NR-PKS PT domains into five major groups with each group corresponding to a unique first-ring cyclization and/or product size: group I, C2−C7 and monocyclic; group II, C2−C7 and bicyclic; group III, C2−C7 and multicyclic; group IV, C4−C9/C2−C11; and group V, C6−C11/C4−C13.[7a] We conducted a Basic Local Alignment Search Tool (BLAST) search for protein sequences with high similarity to that of PhnA PT domain among sequenced fungal genomes. Numerous homologues that share high amino acid identity (50−70%) with the PhnA PT domain were found, all of which are embedded in NR-PKSs of unknown functions and products (Figure S6, SI). Interestingly, several of these homologues were included in the previous phylogenetic analysis and were grouped in group III with other C2−C7-specific PT domains, including that of WA. Repeating the PT phylogenetic analysis after including PhnA PT and other newly sequenced homologues since then led to a clearer classification of them into a separate clade that remains closely related to group III (Figures 7 and S6, SI). This finding is surprising and indicates

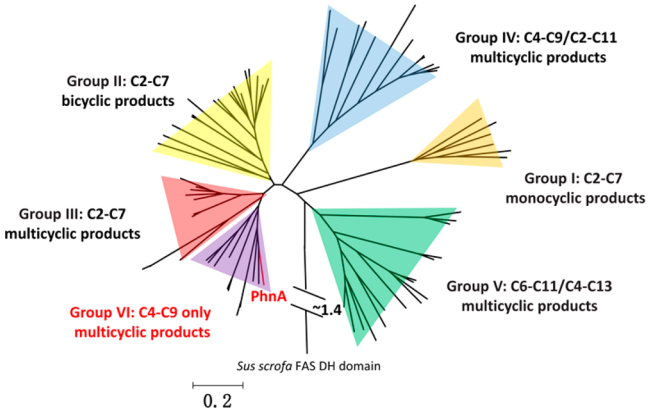

Figure 7. Phylogenetic analysis of the PhnA PT domain with its homologues and previously categorized group I−V PT domains.[7a] Domains were aligned with ClustalW, and the tree was constructed with the neighbor-joining method. Scale bar, 0.2 substitutions per site. The PhnA homologue group is distinct from group IV PT domains and forms a distinct group, VI. This group of PT domains only catalyzes the C4−C9 aldol condensation, and the final products of the NR-PKSs are multicyclic, as in **5**. The PhnA PT domain is indicated with a red line. *Susscrofa* fatty acid synthase DH domain is used as an outgroup in the phylogenetic analysis. A more comprehensive tree is shown in Figure S6 (SI).

that purely sequence based phylogenetic analysis may mask the true cyclization regioselectivity of PT domains. This also indicates that the new group (termed group VI in Figure 7) that includes PhnA is much more closely related to group III than to group IV PT domains, despite sharing the same C4−C9 first-ring cyclization regioselectivity. Indeed, alignment of PhnA PT domain with PT domains from group III showed high sequence similarity, including numerous strictly conserved residues (Figure S23, SI). The PhnA PT domain shares 47% sequence identity and 63% sequence similarity with WA PT but only 30% sequence identity and 49% sequence similarity to CTB1 PT. We can therefore propose that such C4−C9-only PT domains evolved from the group III NR-PKSs via a regioselectivity switch, perhaps controlled by a few residues, instead of from group IV PT domains that require the loss of C2−C11 cyclization capability. The PhnA and WA PT domains can therefore serve as intriguing targets for comparative structural studies toward unmasking residues that are important for regioselectivity control in highly similar domains.

The remaining enzymes encoded in the gene clusters are expected to transform **5** into **3**, as confirmed through the chemical complementation study. These include PhnC (*O*-

DOI: 10.1021/jacs.6b01528
J. Am. Chem. Soc. 2016, 138, 4249−4259

MT), which can methylate C2-OH to stabilize the northern portion of the phenalenone core; PhnF (PrT), which installs the dimethylallyl group at C5; and PhnG (FMO), which can further hydroxylate C6. The precise reaction catalyzed by PhnF, whether it is C7−O prenylation or C6 Friedel−Craft alkylation, is not known and will require additional in vitro biochemical verification. Formation of the fused tetrahydrofuran moiety may require an additional enzyme and may involve those of unassigned function in or immediately adjacent to the gene cluster. Gene clusters containing NR-PKSs identified using PhnA PT domain as the lead were analyzed and compared to the *phn* cluster (Table S4, SI). Each gene cluster contains a close homologue of PhnB in close proximity to the NR-PKS, suggesting that these clusters most likely also synthesize products featuring the phenalenone core (Table S4, SI). Among the strains that contain the identified clusters, the ones that have been reported to produce a phenalenone-containing natural product include funalenone producer *Aspergillus niger* FO-5904[29] and duclauxin **4** producer *Talaromyces stipitatus* ATCC 10500.[30] Funalenone (Figure S1, SI) is the C2-methoxy derivative of **9**, and the structural features are reflected in the *A. niger* gene cluster, which only contains homologues to PhnA, PhnB, PhnC (*O*-MT), and PhnD (Table S4, SI). Similarly, as expected with the structural features of **4**, no homologues of PhnC (*O*-MT), PhnF (PrT), and PhnG (FMO) are found in the *T. stipitatus* gene cluster that contains the PhnA/PhnB pair, while additional enzymes required for the oxidative coupling of two phenalenone cores are present. Therefore, the various combinations of downstream enzymes found in the clusters can serve to predict phenalenone product structures. For example, the clusters from *Cladophialophora psammophila* CBS 110553 and *Cladophialophora bantiana* CBS 173.52 contain all the genes found in the *phn* cluster, inferring the potential to produce compounds that are the same as or closely resembling **3**. Interestingly, the well-studied *Aspergillus terreus* also encodes a *phn*-like gene cluster, although no report of phenalenone isolation has been documented from this strain. On the basis of the gene cluster which lacks PhnF (PrT), one can speculate that this cluster, once transcribed, can produce an unprenylated but C6-hydroxylated derivative of **3**.

In contrast to fungal NR-PKSs, the cyclization regioselectivity of the bacterial aromatic polyketides is entirely controlled by dissociated tailoring enzymes known as cyclases.[2] Cyclases responsible for linear and angular cyclization of the polyketide chain have been well-characterized.[2] Resistomycin produced by *Streptomyces resistomycificus* contains a pentacyclic "discoid" ring system, and is therefore structurally similar to the peri-fused fungal phenalenones. Reconstitution experiments by Hertweck and co-workers demonstrated that formation of the unique discoid fold requires a multienzyme complex that consists of the KS_{α}−KS_{β} pair (RemA−RemB) and three polyketide cyclases (RemF, -L, and -I).[31] It was proposed that the five enzymes form a cage-like environment to promote the S-shaped folding and aldol cyclization of the backbone. Absence of any of the cyclases leads to formation of linear polyketides and other shunt products. The entire ring system in resistomycin may therefore be formed through a series of perhaps concerted aldol condensation steps between intact enolates and carbonyls within the multienzyme complex. This is in sharp contrast to the fungal strategy to generate the phenalenone fold demonstrated here. The involvement of the FMO PhnB was initially unanticipated. However, isolation of the readily formed and stable hemiketal **5** hinted that modification to the THN ring system to promote the C8−C13 reaction must be necessary. The role of PhnB in simultaneously cleaving the pyrone ring and activating the C-3 phenolic oxygen via C-2 hydroxylation, as confirmed through our theoretical calculations, provides another example of the clever use of oxidative enzymes to introduce structural complexity starting from simpler precursors in fungal biosynthetic pathways. Both PhnA PT domain and PhnB add to the biocatalytic toolbox one can access to control rationally polyketide cyclization toward engineered biosynthesis of new aromatic polyketides.

EXPERIMENTAL SECTION

Strains and Culture Conditions. The *P. herquei* strain was obtained from Agriculture Research Service (NRRL 1040) Culture Collection and was used as the parental strain in our study. Both the wild-type and the mutant strains were grown on potato dextrose agar (PDA) (20 g/L dextrose, 4 g/L potato extract, agar 15 g/L) at 28 °C. For gene knockout in *P. herquei*, PDA with 1.2 M sorbitol and 100 μg/mL hygromycin was used for protoplast regeneration and antibiotic resistance selection. *Saccharomyces cerevisiae* strain BJ5464-NpgA (MATα *ura3*-52 *his3*-Δ200 *leu2*-Δ1 *trp1pep4*::HIS3 *prb1*Δ1.6R *can1* GAL) was used. YPD (20 g/L peptone, 10 g/L yeast extract, 20 g/L dextrose) was used for the routine growth of yeast strain BJ5464-NpgA and its derivatives at 30 °C. SD dropout medium was used for selection of plasmids transformed into *S. cerevisiae*. For protein expression under *ADH2* promoter (*ADH 2p*) and pathway reconstitution in *S. cerevisiae*, the appropriate plasmids were introduced into yeast cells as described in Table S5 (SI). The yeast transformants were initially grown in the appropriate SD dropout liquid medium and then transferred to the liquid YPD medium for further culture for 4 days. LB medium was used for culturing *E. coli*. *E. coli* strain DH10b was the host for routine plasmid subcloning and *E. coli* strain BL21(DE3) was used for protein expression and purification for in vitro assay.

***P.herquei* RNA Preparation and Reverse-Transcription Polymerase Chain Reaction (RT-PCR).** Mycelia of *P. herquei* were inoculated in PDB medium, incubated at 28 °C and 200 rpm agitation for 2 days, and collected for lyophilization. The mycelia were ground after freezing with liquid nitrogen and solubilized in Trizol (Invitrogen). One-fifth volume of chloroform was added, and the mixture was vortexed and centrifuged at 15 000 rpm for 15 min. The supernatant was extracted once again with chloroform. RNA was precipitated from the supernatant with ethanol and resuspended in RNase-free water. Genomic DNA was further removed by digestion with RNase-free DNase I (Ambion). RNA was purified by acid phenol (Ambion) extraction and ethanol precipitation. RNA integrity was confirmed by electrophoresis on TBE (Tris−boric acid−EDTA) agarose gel, and the concentration was determined by Nanodrop (Thermo Scientific). cDNA was prepared from 500 ng of total RNA by SuperScript II reverse transcriptase (Invitrogen) with random primers as described by the manufacturer. PCR was performed with Phusion high-fidelity DNA polymerase (New England Biolabs) in the presence of 25 ng of reverse transcribed RNA. Primers are listed in Table S1 (SI).

Plasmid Construction. Primers and plasmids are listed in Tables S1 and S5 (SI), respectively. Yeast expression plasmids pXW02 (LEU2 marker), pXW06 (TRP1 marker), and pXW55 (URA3 marker) were used for construction of the heterologous expression plasmids by in vivo homologous recombination in yeast. All the enzymes were expressed under the strong promoter *ADH 2p*. For polyketide synthase PhnA expression, primers S49 + S50, S51 + S52, S53 + S54, and S55 + S56 were used to amplify four DNA fragments of *phnA* cDNA and were transformed into BJ5464-NpgA with *Spe*I/*Pml*I-digested pXW55 to create the plasmid pGSS1. For polyketide synthase PhnA S2009A expression, primers S49 + S50, S51 + S52, S53 + S54, S55 + S20b, and S21b + S56 were used to amplify five DNA fragments from *phnA* cDNA, by mutating the putative active site (GWSAG)

DOI: 10.1021/jacs.6b01528
J. Am. Chem. Soc. 2016, 138, 4249−4259

serine (S2009A) in PhnA, and were transformed into BJ5464-NpgA with *Spe*I/*Pml*I-digested pXW55 to create the plasmid pGSS2. For TE-less PhnA expression, primers S49 + S50, S51 + S52, S53 + S54, and S55 + S22b were used to amplify four DNA fragments from *phnA* cDNA, by deletion of the 700 bp TE/CLC domain in PhnA, and were transformed into BJ5464-NpgA with *Spe*I/*Pml*I-digested pXW55 to create the plasmid pGSS3. Yeast competent cell preparation and transformation were performed with an S.c. EasyComp transformation kit (Invitrogen) according to the manufacture's protocols. Yeast plasmids were prepared by a Zymoprep Yeast Plasmid Miniprep kit (Zymo Research) and transformed into *E. coli* strain DH10b for propagation. To construct the plasmids for gene knockout in *P. herquei* based on the split-marker strategy, the plasmid pAN7-14 was used as the template to amplify the *hph* upstream fragment with primers hph-up F and hph-up R and the *hph* downstream fragment with primers hph-dn F and hph-dn R. Both fragments were digested with *Not*I/*Sac*II and *Sac*I/*Not*I, respectively, and ligated to T-vector pTA2 to generate plasmids pXM11 and pXM12. The upstream DNA fragments of the KS region of *phnA* and *phnB* were amplified with primer pairs S45 + S46 and S77 + S78. The PCR products were digested with *Hin*dIII/*Not*I (for KO of the KS region of *phnA*) or *Cla*I/*Not*I (for KO of the *phnB* gene) and ligated to the *Hin*dIII/*Not*I (for KO of the KS region of *phnA*) or *Cla*I/*Not*I (for KO of the *phnB* gene) site of pXM11 to afford plasmids pGSS6 and pGSS8, respectively. Meanwhile, the downstream DNA fragments of the KS region of *phnA* and *phnB* were amplified with primer pairs S47 + S48 and S79 + S80 digested with *Hin*dIII/*Not*I (for KO of the KS region of phnA) or *Cla*I/*Not*I (For KO of the *phnB* gene) and ligated to the *Hin*dIII/*Not*I (for KO of the KS region of *phn*A) or *Cla*I/*Not*I (for KO of the *phnB* gene) site of pXM12 to create plasmids pGSS7 and pGSS9, respectively.

Construction of *P. herquei* Mutants. All the mutants were constructed in *P. herquei* based on the hygromycin split-marker strategy.[32] The upstream split-marker DNA for KO of the KS region of *phnA* and *phnB* were amplified with S45 + S2 and S77 + S2 from plasmids pGSS6 and pGSS8, respectively. The downstream split-marker DNA for KO of the KS region of *phnA* and *phnB* were amplified with S48 + S3 and S80 + S3 from plasmids pGSS7 and pGSS9, respectively. The PCR products were gel purified and dissolved in STC buffer. Split-marker DNA was introduced into *P. herquei* by protoplast transformation. *P. herquei* spores were collected on PDA (Fluka) for 4 days at 28 °C and induced to young germ tubes in PDB (Fluka) at 25 °C for 7 h with 200 rpm agitation. Mycelia were collected, washed twice with the osmotic medium (1.2 M $MgCl_2$, 10 mM sodium phosphate, pH 5.8), and resuspended in the enzyme cocktail solution (3 mg/mL lysing enzymes, 3 mg/mL yatalase in osmotic medium) at 30 °C for overnight. After washing twice with STC buffer, protoplasts were gently mixed with DNA and incubated for 1 h on ice. One milliliter of PEG 4000 solution (60% PEG 4000, 50 mM $CaC1_2$, 50 mM Tris-HCI, pH 7.5) was added to 100 μL of protoplast mixture, and the mixture was incubated at room temperature for 30 min and plated on the regeneration selection medium (PDA, 1.2 M sorbitol, 100 μg/mL hygromycin B). After incubation at room temperature for about 4 days, the transformants were inoculated on PDB medium with stationary incubation for about 1 week to confirm the genotype by PCR after preparation of the genomic DNA.

Yeast Reconstitution of Phenalenone Biosynthesis Pathway. *S. cerevisiae* strain BJ5464-NpgA was transformed with appropriate plasmid(s) as described in Table S5 (SI). Yeast cells containing transformed plasmid(s) were initially cultured in the dropout medium overnight and transferred to 50 mL of liquid YPD medium for an additional 4-day culture. Extracted samples from approximately 0.5 mL of culture were loaded for LC−MS analysis.

Chemical Complementation Studies. For chemical complementation of the Δ*phnA* strain of *P. herquei* with compounds (solubilized in DMSO), spores of Δ*phnA* were inoculated on a PDA plate, together with 10 μg/mL compounds **5** and **9**, and further cultured for 3 days at 28 °C. The mycelia and medium were extracted for LC−MS analysis.

LC−MS Analysis. Cultures of *P. herquei*, *S. cerevisiae*, or *E. coli* cells were extracted with methanol:ethyl acetate (10:90). After brief centrifugation, the supernatant organic phase was dried and solubilized in methanol for LC−MS injection. All LC−MS analyses were performed on a Shimadzu 2020 EVLC-MS (Phenomenex Luna, 5 μm, 2.0 × 100 mm, C18 column) using positive and negative mode electrospray ionization with a linear gradient of 5−95% acetonitrile (MeCN)−H_2O in 15 min followed by 95% MeCN for 5 min with a flow rate of 0.3 mL/min.

Protein Expression and Purification of PhnB from *E. coli* Strain BL21 (DE3). The expression plasmid pGSS30 was transformed into *E. coli* strain BL21 (DE3) for expression of PhnB. Cells in LB medium (1 L) supplemented with kanamycin (35 mg/L) inoculated with BL21(DE3)/pGSS30 were grown to an OD_{600} of 0.6. Protein expression was then induced with 0.12 mM of isopropylthio-D-galactoside (IPTG, Sigma-Aldrich), followed by further incubation with shaking at 250 rpm at 16 °C for 16 h. All of the enzyme purification steps were conducted at 4 °C using Nickel−NTA affinity chromatography following standard protocols. Purified proteins were concentrated and exchanged into buffer C (50 mM Tris-HCl, pH 7.9, 50 mM NaCl, and 5% glycerol) with Centriprep filters (Amicon). The protein was stored in buffer C at −80 °C. Protein concentration was determined by Bradford assay using bovine serum albumin as a standard.

Protein Expression and Purification of PhnA from *S. cerevisiae* Strain BJ5464-NpgA. The expression plasmid pGSS1was transformed into *S. cerevisiae* strain BJ5464-NpgA for expression of PhnA. Cells in YPD medium inoculated with BJ5464-NpgA/pGSS1 were grown for 3 days for protein expression. *S. cerevisiae* cells were harvested by centrifugation (5000 rpm, 15 min, 4 °C), resuspended in 300 mL yeast lysis buffer, and lysed with sonication on ice. Cellular debris was removed by centrifugation (17 000*g*, 1 h, 4 °C). FLAG-tagged proteins were purified by using Anti-FLAGM1 agarose affinity gel (Sigma-Aldrich), following the supplied protocols. Purified proteins were concentrated, buffer exchanged into 50 mM potassium phosphate buffer (pH 7.0) with 10% glycerol, concentrated, aliquoted, and flash frozen. Protein concentrations were determined using the Bradford dye-binding assay (Bio-Rad).

In Vitro Activity Assay for PhnB and PhnA. PhnB activity was assayed by monitoring the conversion of substrates into products, as analyzed by LC−MS. A typical 100 μL assay solution contained 100 mM potassium phosphate buffer (pH 7.5), 4 mM NADPH (Sigma-Aldrich), 20 μM FAD (Sigma-Aldrich), 5 μM PhnB, and 1 mM **5**. The reactions was performed at 25 °C and quenched with ethyl acetate. For the in vitro activity assay of PhnA, a typical 100 μL assay solution contained 100 mM phosphate buffer and 2 mM malonyl coenzyme A lithium salt. The reaction was performed at 28 °C and quenched with an equal volume of methanol. Protein precipitate from the reactions was removed by centrifugation. The supernatant was further extracted with 500 μL of ethyl acetate, dried, redissolved in 30 μL of DMSO, and then analyzed by LC−MS. LC−MS analyses were performed on a Shimadzu 2020 EV LC-MS (Kinetex 1.7 μm C18 100 Å, LC column 100 × 2.1 mm) using positive and negative mode electrospray ionization with a linear gradient of 5−95% MeCN−H_2O in 15 min followed by 95% MeCN for 3 min with a flow rate of 0.3 mL/min.

Chemical Analysis and Compound Isolation. From yeast, the ethyl acetate extract from 4 L of YPD liquid medium was evaporated to dryness to yield the crude extract. From *P. herquei*, the acetone extract from 2 L of PDA solid agar extract of mutant was evaporated to dryness and partitioned between ethyl acetate/H_2O three times. To purify the desired compound, crude extracts were separated by Sephadex-LH20, reverse phase-C18, and additional HPLC steps as required. Generally, the crude extract obtained from the yeast culture or from *P. herquei* cultivated on the PDA solid agar plates was submitted to Sephadex-LH20 eluted with methanol. After analysis by LC−MS, the fractions containing the target compound were combined and then submitted to separation by an ISCO-CombiFlash Rf 200 (Teledyne Isco, Inc.) with a reverse-phase C18 column eluted by a gradient of methanol and water. After analysis by LC−MS, the fractions containing the target compound were combined and further

DOI: 10.1021/jacs.6b01528
J. Am. Chem. Soc. 2016, 138, 4249−4259

purified by semipreparative HPLC using a C18 reverse-phase column. The purity of each compound was checked by LC−MS, and the structure was confirmed by NMR. ^{1}H, ^{13}C, and 2D NMR spectra were obtained using DMSO-d_6 or CD_3OD as solvent on a Bruker AV500 spectrometer with a 5 mm dual cryoprobe at the UCLA Molecular Instrumentation Center.

Purification of 9. The crude extract containing **9** was obtained from a 4 day culture of *S. cerevisiae* BJ5464-NpgA expressing PhnA and PhnB in YPD broth. The crude extract was subjected to HPLC chromatography on a Phenomenex Luna column (250 × 10 mm, 5 μm, 40 °C, flow 4 mL/min) eluted with an isocratic wash of 30% MeCN in water for 20 min to yield a subfraction. The subfraction was further subjected to HPLC chromatography on Phenomenex Luna column (250 × 10 mm, 5 μm, 40 °C, flow 4 mL/min) with an isocratic wash of 50% MeOH in water for 20 min. The purified fraction was cooled immediately on ice. The solvent was quickly removed under reduced pressure, and the remaining water was frozen and lyophilized to yield 1.5 mg of **9**.

Computational Methods. Quantum mechanical calculations were performed using Gaussian 09 (Revision D.01).[33] All geometries were optimized using B3LYP[34] and the 6-31G(d) basis set. Single-point energies were calculated using M06-2X[35] and the def2-TZVPP basis set on the B3LYP-optimized structured. All the results have been calculated in the gas phase at 298 K. Computed structures were illustrated with CYLview, ver. 1.0b (C. Y. Legault, Université de Sherbrooke, 2009;http://www.cylview.org).

■ ASSOCIATED CONTENT

Supporting Information

The Supporting Information is available free of charge on the ACS Publications website at DOI: 10.1021/jacs.6b01528.

Spectroscopic information, computational data and additional experimental details (Tables S1−S8 and Figures S1−S52) (PDF)

■ AUTHOR INFORMATION

Corresponding Authors

*houk@chem.ucla.edu

*yitang@ucla.edu

Notes

The authors declare no competing financial interest.

■ ACKNOWLEDGMENTS

This work was supported by the NIH (1DP1GM106413 and 1R01GM085128 to Y.T.) and the NSF (CHE-1361104 to K.N.H.). Computational resources were provided by the UCLA Institute for Digital Research and Education (IDRE) and the Extreme Science and Engineering Discovery Environment (XSEDE), which is supported by the NSF (OCI-1053575).

■ REFERENCES

(1) (a) Cox, R. J. *Org. Biomol. Chem.* **2007**, *5*, 2010. (b) Chooi, Y. H.; Tang, Y. *J. Org. Chem.* **2012**, *77*, 9933.

(2) Zhou, H.; Li, Y.; Tang, Y. *Nat. Prod. Rep.* **2010**, *27*, 839.

(3) Crawford, J. M.; Dancy, B. C. R.; Hill, E. A.; Udwary, D. W.; Townsend, C. A. *Proc. Natl. Acad. Sci. U. S. A.* **2006**, *103*, 16728.

(4) Crawford, J. M.; Korman, T. P.; Labonte, J. W.; Vagstad, A. L.; Hill, E. A.; Kamari-Bidkorpeh, O.; Tsai, S.-C.; Townsend, C. A. *Nature* **2009**, *461*, 1139.

(5) Ma, Y.; Smith, L. H.; Cox, R. J.; Beltran-Alvarez, P.; Arthur, C. J.; Simpson, F. R. S. T. *ChemBioChem* **2006**, *7*, 1951.

(6) Fujii, I.; Watanabe, A.; Sankawa, U.; Ebizuka, Y. *Chem. Biol.* **2001**, *8*, 189.

(7) (a) Li, Y.; Xu, W.; Tang, Y. *J. Biol. Chem.* **2010**, *285*, 22764. (b) Zhang, W.; Li, Y.; Tang, Y. *Proc. Natl. Acad. Sci. U. S. A.* **2008**, *105*, 20683. (c) Crawford, J. M.; Thomas, P. M.; Scheerer, J. R.; Vagstad, A. L.; Kelleher, N. L.; Townsend, C. A. *Science* **2008**, *320*, 243.

(8) Cacho, R. A.; Chooi, Y. H.; Zhou, H.; Tang, Y. *ACS Chem. Biol.* **2013**, *8*, 2322.

(9) (a) Ma, S. M.; Zhan, J.; Xie, X.; Watanabe, K.; Tang, Y.; Zhang, W. *J. Am. Chem. Soc.* **2008**, *130*, 38. (b) Korman, T. P.; Crawford, J. M.; Labonte, J. W.; Newman, A. G.; Wong, J.; Townsend, C. A.; Tsai, S. C. *Proc. Natl. Acad. Sci. U. S. A.* **2010**, *107*, 6246.

(10) Ma, S. M.; Zhan, J.; Watanabe, K.; Xie, X.; Zhang, W.; Wang, C. C.; Tang, Y. *J. Am. Chem. Soc.* **2007**, *129*, 10642.

(11) (a) Newman, A. G.; Vagstad, A. L.; Storm, P. A.; Townsend, C. A. *J. Am. Chem. Soc.* **2014**, *136*, 7348. (b) Xu, Y.; Zhou, T.; Zhou, Z.; Su, S.; Roberts, S. A.; Montfort, W. R.; Zeng, J.; Chen, M.; Zhang, W.; Lin, M.; Zhan, J.; Molnár, I. *Proc. Natl. Acad. Sci. U. S. A.* **2013**, *110*, 5398. (c) Vagstad, A. L.; Newman, A. G.; Storm, P. A.; Belecki, K.; Crawford, J. M.; Townsend, C. A. *Angew. Chem., Int. Ed.* **2013**, *52*, 1718.

(12) Elsebai, M. F.; Saleem, M.; Tejesvi, M. V.; Kajula, M.; Mattila, S.; Mehiri, M.; Turpeinen, A.; Pirttila, A. M. *Nat. Prod. Rep.* **2014**, *31*, 628.

(13) (a) Frost, D. A.; Halton, D. D.; Morrison, G. A. *J. Chem. Soc., Perkin Trans. 1* **1977**, 2443. (b) Narasimhachari, N.; Vining, L. C. *J. Antibiot.* **1972**, *25*, 155. (c) Cao, P.; Yang, J.; Miao, C. P.; Yan, Y.; Ma, Y. T.; Li, X. N.; Zhao, L. X.; Huang, S. X. *Org. Lett.* **2015**, *17*, 1146.

(14) (a) Vertesy, L.; Kurz, M.; Li, Z.; Toti, L. Patent US7253206 B2, 2007. (b) Elsebai, M. F.; Kehraus, S.; Lindequist, U.; Sasse, F.; Shaaban, S.; Gutschow, M.; Josten, M.; Sahl, H.-G.; Konig, G. M. *Org. Biomol. Chem.* **2011**, *9*, 802. (c) Shiomi, K.; Matsui, R.; Isozaki, M.; Chiba, H.; Sugai, T.; Yamaguchi, Y.; Masuma, R.; Tomoda, H.; Chiba, T.; Yan, H.; Kitamura, Y.; Sugiura, W.; Ōmura, S.; Tanaka, H. *J. Antibiot.* **2005**, *58*, 65.

(15) (a) Simpson, T. J. *J. Chem. Soc., Chem. Commun.* **1976**, 258. (b) Simpson, T. J. *J. Chem. Soc., Perkin Trans. 1* **1979**, 1233.

(16) Nazir, M.; El Maddah, F.; Kehraus, S.; Egereva, E.; Piel, J.; Brachmann, A. O.; Konig, G. M. *Org. Biomol. Chem.* **2015**, *13*, 8071.

(17) Suga, T.; Yoshioka, T.; Hirata, T.; Aoki, T. *Chem. Lett.* **1981**, 1063.

(18) Li, R.; Zhu, H.; Ruan, J.; Qian, W.; Fang, X.; Shi, Z.; Li, Y.; Li, S.; Shan, G.; Kristiansen, K.; Yang, H.; Wang, J.; Li, S.; Wang, J. *Genome Res.* **2010**, *20*, 265.

(19) Medema, M. H.; Blin, K.; Cimermancic, P.; de Jager, V.; Zakrzewski, P.; Fischbach, M. A.; Weber, T.; Takano, E.; Breitling, R. *Nucleic Acids Res.* **2011**, *39*, W339.

(20) (a) Ma, S. M.; Li, J. W.; Choi, J. W.; Zhou, H.; Lee, K. K.; Moorthie, V. A.; Xie, X.; Kealey, J. T.; Da Silva, N. A.; Vederas, J. C.; Tang, Y. *Science* **2009**, *326*, 589. (b) Lee, K. K.; Da Silva, N. A.; Kealey, J. T. *Anal. Biochem.* **2009**, *394*, 75.

(21) Rugbjerg, P.; Naesby, M.; Mortensen, U. H.; Frandsen, R. JN. *Microb. Cell Fact.* **2013**, *12*, 31.

(22) An, J. H.; Kim, Y. S. *Eur. J. Biochem.* **1998**, *257*, 395.

(23) Newman, A. G.; Vagstad, A. L.; Belecki, K.; Scheerer, J. R.; Townsend, C. A. *Chem. Commun.* **2012**, *48*, 11772.

(24) Lin, H. C.; Tsunematsu, Y.; Dhingra, S.; Xu, W.; Fukutomi, M.; Chooi, Y. H.; Cane, D. E.; Calvo, A. M.; Watanabe, K.; Tang, Y. *J. Am. Chem. Soc.* **2014**, *136*, 4426.

(25) Gagne, S. J.; Stout, J. M.; Liu, E.; Boubakir, Z.; Clark, S. M.; Page, J. E. *Proc. Natl. Acad. Sci. U. S. A.* **2012**, *109*, 12811.

(26) Young, I. G.; Stroobant, P.; Macdonald, C. G.; Gibson, F. *J. Bacteriol.* **1973**, *114*, 42.

(27) Ishikawa, Y.; Morimoto, K.; Iseki, S. *J. Am. Oil Chem. Soc.* **1991**, *68*, 666.

(28) Walsh, C. T.; Wencewicz, T. A. *Nat. Prod. Rep.* **2013**, *30*, 175.

(29) Inokoshi, J.; Shiomi, K.; Masuma, R.; Tanaka, H.; Yamada, H.; Omura, S. *J. Antibiot.* **1999**, *52*, 1095.

(30) (a) Nierman, W. C.; Fedorova-Abrams, N. D.; Andrianopoulos, A. *Genome Announc.* **2015**, *3*, e01559-14. (b) Frisvad, J. C.; Filtenborg, O.; Samson, R. A.; Stolk, A. C. *Antonie van Leeuwenhoek* **1990**, *57*, 179.

DOI: 10.1021/jacs.6b01528
J. Am. Chem. Soc. 2016, 138, 4249−4259

(31) (a) Fritzsche, K.; Ishida, K.; Hertweck, C. *J. Am. Chem. Soc.* **2008**, *130*, 8307. (b) Jakobi, K.; Hertweck, C. *J. Am. Chem. Soc.* **2004**, *126*, 2298.
(32) Punt, P. J.; Dingemanse, M. A.; Kuyvenhoven, A.; Soede, R. D. M.; Pouwels, P. H.; van den Hondel, C. A. M. J. J. *Gene* **1990**, *93*, 101.
(33) Frisch, M. J.; et al. *Gaussian 09*, Revision D.01; Gaussian, Inc.: Wallingford, CT, 2009.
(34) Becke, A. D. *J. Chem. Phys.* **1993**, *98*, 5648.
(35) Zhao, Y.; Truhlar, D. G. *Theor. Chem. Acc.* **2008**, *120*, 215.

DOI: 10.1021/jacs.6b01528
J. Am. Chem. Soc. 2016, 138, 4249−4259